ASSIGNING PROBABILITIES TO QUALITATIVE DYNAMICS OF GENE REGULATORY NETWORKS

L. IRONI[1] AND E. LANZARONE[2]

[1]IMATI-CNR "Enrico Magenes", via Ferrata 1, I-27100 Pavia, Italy
[2]IMATI-CNR "Enrico Magenes", via Bassini 15, I-20133 Milano, Italy

Abstract.
Mathematical and computational modeling frameworks play the leading role in the analysis and prediction of the dynamics of gene regulatory networks. The literature abounds in various approaches, all of which characterized by strengths and weaknesses. Among the others, ODE models give a more general and detailed description of the network structure. But, analytical computations might be prohibitive as soon as the network dimension increases, and numerical simulation could be nontrivial, time-consuming and very often impracticable as precise and quantitative information on model parameters are frequently unknown and hard to estimate from experimental data. Last but not least, they do not account for the intrinsic stochasticity of regulation.

In the present paper we consider a class of ODE models with stochastic parameters. The proposed method separates the deterministic aspects from the stochastic ones. Under specific assumptions and conditions, all possible trajectories of an ODE model, where incomplete knowledge of parameter values is symbolically and qualitatively expressed by initial inequalities only, are simulated in a single run from an initial state. Then, the occurrence probability of each trajectory, characterized by a sequence of parameter inequalities, is computed by associating probability density functions with network parameters.

As demonstrated by its application to the gene repressilator system, the method seems particularly promising in the design of synthetic networks.

Key words.
Gene regulatory networks, nonlinear ODE models, stochastic parameters, qualitative simulation.

AMS subject classifications. 34C60, 34E15, 60H10, 92B99

1. Introduction. The concentration levels and the temporal patterns of gene products, crucial to both developmental and housekeeping processes, are controlled by networks of mutual regulatory interactions between molecular species, e.g., genes, RNAs, proteins, etc., the so-called Gene Regulatory Networks (GRN). Innovative experimental technologies have made their disclosure possible and revealed the extreme complexity of their underlying structures. Thus, for the comprehension and prediction of the dynamics of these networks, mathematical models combined with computational analyzers and/or simulators are essential and valuable tools [1].

A variety of frameworks that support both gene network modeling and simulation have been developed [4, 16, 21]. All proposed methods have particular goals, strengths and weaknesses, and capture network dynamics at different resolutions, both discrete and continuous. They also differ on how they model response functions in transcription regulation, for example Heaviside response functions, Hill response functions, mass action law dynamics, and Michaelis-Menten response functions. There exist pure deterministic models as well as stochastic models. There is no general agreement in the literature on how to model transcription regulation in the most correct way but the usefulness of one or the other of these approaches to study a specific network depends on applicability, generalization and modeling tasks.

The most detailed relationships between stochasticity and gene regulation are explained in several scenarios by single-molecule level models [23]. GRNs can be considered as systems of coupled chemical reactions, and, under the assumption of spatial homogeneity, the stochastic process underlying them can be modeled as a

Markov process. Two main approaches to modeling stochastic events exist: stochastic differential equations and stochastic simulation algorithms [21, 25]. Stochastic differential models are mainly based on variations of the chemical master equation. These models capture stochasticity quite well but they are too complex to be solved analytically and are mostly intractable, even numerically, when a large number of molecules are considered. Stochastic simulation algorithms (SSA), *i.e.*, the Gillespie's algorithm and its variants, perform numerical simulation of the Markov process they describe [8, 9]. The SSA algorithms give a good approximation of the chemical master equation. The bottleneck of these methods lies in the large computation time of their application because they simulate every individual reaction. To speed up SSA, there are several different implementation strategies, among those we mention the τ-leaping one. It leaps over many reactions in one time step [10] and gives the better performance in terms of efficiency. But, in the words of [3]: *Approximations of the τ-leaping method can sometimes cause unphysical results, such as negative number of molecules*. Practical but complex implementation strategies aiming at balancing accuracy with efficiency of the τ-leaping method have been given in the literature [3].

In a deterministic framework, a general and detailed description of the dynamics of gene regulatory networks is provided by phenomenological models formalized by Ordinary Differential Equations (ODE). In theory, ODE models have a great predictive potential, but, in practice, they are currently applicable to only a few systems. A numerical investigation of large networks could be nontrivial, time consuming and often impracticable as it requires precise knowledge on kinetic parameters, scarcely available for the biochemical reaction mechanisms underlying gene regulatory interactions and often not identifiable from experimental data. However, where the network of interactions is complex and parameter values are not known with any precision, a qualitative study of these models is still valuable for understanding potential dynamical behavior and for disclosing and developing "principles" relating network structure to dynamics. To support qualitative analysis and simulation, computational tools are necessary as the analysis easily gets prohibitive as soon as the network dimension increases. Only few computational tools are currently available. One of them, called GNA, provides automated qualitative analysis of models of GRNs with Heaviside response functions, *i.e.*, Piecewise-Linear ODE models [5]. In this tool the analysis is based on the Filippov approach, but, problems can arise with non-existence or non-uniqueness of solutions, some of which are spurious [22].

An alternative computational framework considers ODE models that capture the intrinsic nonlinearity and temporal multi-scale of GRN dynamics by using steep sigmoid response functions. The simulation algorithm of the solutions of these models is based on sound rules established by the results given in [14], that give sufficient conditions ensuring the applicability of the singular perturbation method under specific biologically reasonable assumptions. The resulting tool provides sound and complete predictions [15], *i.e.*, in a *single run*, it provides *all possible dynamics* of nonlinear and temporal multi-scale dynamics of GRN, where each predicted trajectory is characterized by delimited ranges of parameter values as well as by its qualitative dynamical property, e.g., stable, cyclic or spiraling solution. Although limitedly to a specific class of models, the latter computational framework holds the potential power to predict either the full range of network dynamics under different conditions or the dynamical changes in correspondence of network failures and/or extreme conditions. It may challenge several fields, from biotechnology to medicine, and may play a crucial role in the comprehension of natural biological systems and, in particular, in the design and

construction of a synthetic network that exhibits a desired behavior, e.g., sustained oscillations [2, 7, 11, 12, 17, 18, 27].

In this paper we present a method to enable the above computational tool to assign a probability of occurrence to each of the predicted trajectories. We take stochasticity into account by considering ODE models with steep sigmoid response functions where the network structure along with gene interactions are given, and the network uncertainty is expressed by fluctuations in parameter values only. This assumption allows us to keep the deterministic aspects of model predictions separated from the stochastic ones with the consequent advantage of getting sustainable computational costs. This in contrast with traditional approaches to solve ODEs with stochastic coefficients for which the computational effort might be very high and dramatically increase with the network dimension due to the heavy computation required for deriving the solutions directly from the nonlinear stochastic differential model [19, 24]. We remark that, in the traditional approaches, each stochastic trajectory is determined by averaging several trajectories, each of them obtained by extracting a value for each parameter from its density function at every integration step. Thus, the computational effort refers to the repeated computation needed for each stochastic trajectory, whereas in our method it refers to the generation of all the qualitative distinctions of the dynamics together with the computation of their probability of occurrence.

In outline, first the method derives all symbolic/qualitative predictions of the network dynamics from the ODE model together with initial conditions, where model parameter values are given in terms of ranges of values symbolically and qualitatively expressed by inequalities. Each trajectory in the solution tree is associated with sequence of inequalities and occurs if all the inequalities are satisfied. The occurrence probability of a trajectory is then given by assigning probability density functions to the network parameters and, then, by calculating the probability that the whole sequence of inequalities is satisfied. Assigning probabilities to admissible trajectories is an important added value to the simulator as it makes it effectively applicable to realistic contexts, especially in the design of a synthetic network that implements a particular function or behavior where the uncertainty about the values of parameters that characterize the interactions between different components should be delimited.

The method works independently of the type of distributions assigned to each parameter. Probability distributions must be in agreement with modeling assumptions and represent the available knowledge on the network: the more complete is the knowledge of a parameter value the lower should be the variance of its distribution. Then, the method enables us to mix different levels of knowledge on parameters. Some may be completely unknown, some known with a relevant uncertainty, and others well known. In terms of network structure this means that we can infer the dynamics of a network that can include sub-networks with different degrees of knowledge, for example a large network including some well-studied small networks. This might favour a process to incrementally increase knowledge of gene regulatory networks, both natural and synthetic, starting from the analysis of its small sub-networks.

The organization of the paper is as follow: Sect. 2 presents the mathematical background underlying the adopted qualitative simulation algorithm of a class of ODEs conventionally considered in the literature as a model framework for GRNs. Sect. 3 is the core of the paper and is devoted to the method for assigning probabilities to the simulation outcome, namely all the possible predicted trajectories with given initial conditions. The application potential of the method in the context of synthetic network design is given in Sect. 4 by applying the method to the repressi-

lator system [7]. Finally, Sect. 5 contains a discussion and our concluding remarks. For the sake of completeness, we recall the Monte-Carlo integration method in the Appendix.

2. Background: qualitative simulation of a class of dynamical models. For the sake of clarity and completeness, we briefly recall the basic assumptions, definitions and methods underlying a qualitative simulation algorithm of phenomenological models of the dynamics of gene regulatory networks [14]. Such models are conventionally given in the literature by the equations:

$$\dot{x_i} = F_i(Z) - \gamma_i x_i, \qquad i = 1, \ldots, n, \tag{2.1}$$

where $x_i \in \mathbb{R}_+$ denotes the concentration of gene product number i. Each equation contains a linear degradation term $-\gamma_i x_i$ with relative rate $\gamma_i > 0$, and a nonlinear production one $F_i(Z)$, where $Z = \{Z_{ij}\}$ is the set of nonlinear steep sigmoid functions that rule regulation. More precisely, $Z_{ij} : \mathbb{R}_+ \to [0, 1]$ is a function of the variable x_i that continuously switches from 0 to 1 around a certain threshold concentration θ_{ij}, with a steep rise q. Let us observe that we consider the inverse steepness parameter $0 < q \ll 1$, such that the more the value of q is small, the more the state change around the threshold is steep. As we consider phenomenological deterministic models of biochemical interaction chains, a steep sigmoid function is conveniently modeled by the Hill function $\frac{x^{1/q}}{x^{1/q}+\theta^{1/q}}$, with q small. We assume that the m_i threshold values θ_{ij} for any x_i are ordered such that $\theta_{ij} < \theta_{ik}$ if $j < k$, and we define $\theta_{i0} = 0$, for any i. The term $F_i(Z)$, frequently composed by algebraic equivalence of Boolean functions, is mathematically expressed by a multilinear polynomial in the variables Z_{ij} with real-valued production rate k_{il}, where l indicates the l-th interaction in the network that contributes to the dynamics of x_i, and multilinear means linear in each variable.

The m_i hyper-planes $x_i = \theta_{ij}$ induce a natural partition of the phase-plane into qualitatively distinct rectangular domains Δ, that we call *regular* and *switching* domains.

Let us indicate with δ a positive number such that 2δ is smaller than the difference between any two neighboring thresholds. The steepness parameter q associated with the response function Z_{ij} determines a narrow band of width $2\delta > 0$ around θ_{ij}, where $\delta \to 0$ when $q \to 0$. A *regular domain* is a connected rectangular domain where $|x_i - \theta_{ij}| > \delta$ for all i and j. In a regular domain all Z_{ij} are close to 0 or 1. Thus, for each Z_{ij} we define a variable B_{ij} such that $B_{ij} = 0$ if $x_i < \theta_{ij} - \delta$ and $B_{ij} = 1$ if $x_i > \theta_{ij} + \delta$.

To define a switching domain we first distinguish the network variables x_i in regular variables x_r and switching variables x_s, where $r \in R$, $s \in S$, and $R \cup S = N = \{1, 2, \cdots, n\}$. A variable x_i is called *switching*, when it assumes values such that $|x_i - \theta_{ij}| \leq \delta$ for some non-null j. Otherwise, it is called *regular*. We will denote the whole set of variables, the set of switching and regular variables by x_N, x_S, and x_R, respectively. Each switching domain is characterized by the sets x_S and x_R, as well as by the set θ_S that contains one threshold θ_{s,j_s} for each $x_s \in x_S$. Thus, if we let I_r be a non-negative integer, a switching domain is such that $|x_s - \theta_{s,j_s}| < \delta$ for all $s \in S$, and $\theta_{r,I_r} + \delta < x_r < \theta_{r,I_r+1} - \delta$ for each r in R. A switching domain defined in this way will be denoted $\Delta(S, R, \theta_S, I_R)$. As shown in Fig. 2.1, in the phase space partition there exist domains where either S or R, and consequently θ_S or I_R, are empty.

2.1. Multi-scale dynamics in a domain. In a domain $\Delta(S, R, \theta_S, I_R)$ the spatial variation of a switching variable x_s is very small, and precisely amounts to

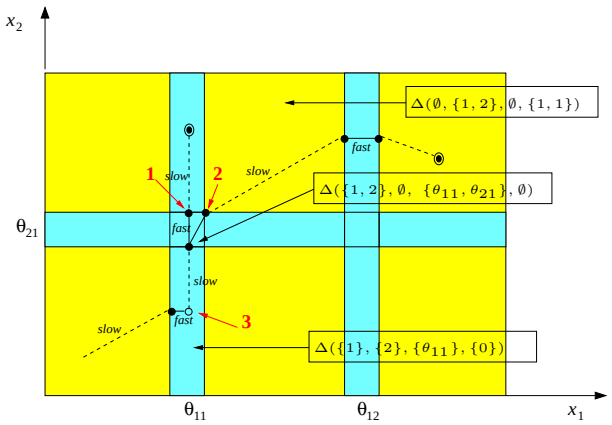

FIG. 2.1. *Idealized dynamics of systems* (2.1) *with* $n = 2$ *in the phase space partitioned into domains* Δ. *Regular domains are yellow colored and switching domains are blue colored. In the figure, definitions of some* Δ*s are given on the right side. Continuous and dashed lines indicate fast and slow motion, respectively. Both motions may occur in domains where* $S \neq \emptyset$ *and* $R \neq \emptyset$. *The double circles denote stable points. The filled circles denote arrival/departure points on the boundaries of domains: in* $\Delta(\{1,2\}, \emptyset, \{\theta_{11}, \theta_{21}\}, \emptyset)$ *when all the components of the exit point (labeled as 2) take integer values only the dynamics enters a regular domain; when the components of the departure point (labeled as 1) take non-integer and integer value the dynamics slides towards either the next threshold or the focal point. The entrance/exit points refer to the switching components of the arrival/departure points only, and the empty circle denotes an exit point (labeled as 3) from the switching cross section, from which the slow motion continues towards the boundary of the domain.*

2δ, while the corresponding Z_s jumps from nearly 0 to nearly 1 in a very short time interval. On the contrary, the response functions Z_R and $Z_{S'}$ associated, respectively, with regular or switching variables that assume values far from the thresholds in Δ take values either nearly 0 or nearly 1 on larger time intervals. This means that regulation dynamics goes *faster* than the dynamics of regular or off-threshold variables. To mathematically highlight this phenomenon, we study the dynamics of x_s variables in the reference system of the variables Z. Thus, in Δ (2.1) can be rewritten as:

$$\begin{aligned} q\dot{Z}_s &= D_s[F_s(Z_S, Z_{S'}, Z_R) - \gamma_s x_s], \qquad s \in S, \\ \dot{x}_r &= F_r(Z_S, Z_{S'}, Z_R) - \gamma_r x_r, \qquad r \in R, \end{aligned} \tag{2.2}$$

where D_s stems from the derivative of $\frac{dZ_s}{dx_s}$. In the case of the Hill function $q\frac{dZ_s}{dx_s} = \frac{Z_s(1-Z_s)}{x_s}$.

In accordance with standard singular perturbation method, the fast motion is studied in the fast timescale $\tau = t/q$ that leads to:

$$\begin{aligned} Z_s' &= D_s[F_s(Z_S, Z_{S'}, Z_R) - \gamma_s \theta_s], \qquad s \in S, \\ x_r' &= q[F_r(Z_S, Z_{S'}, Z_R) - \gamma_r x_r], \qquad r \in R, \end{aligned} \tag{2.3}$$

where the prime denotes the derivative with respect to τ. In the limit $q \to 0$, (2.3) simplifies to the *boundary layer equation*:

$$Z_s' = D_s^0[F_s(Z_S, B_{S'}, B_R) - \gamma_s \theta_s], \qquad s \in S, \tag{2.4}$$

where $D_s^0 = \lim_{q \to 0} D_s$, and $B_{S'}$ and B_R are the sets of Boolean values for the switching components outside Δ and the regular components, respectively. Thus, in

the limit, the term F_s in (2.4) depends only on variables Z_s, and fast and slow motion can be studied separately.

In the limit, during the fast motion of Z_S, the regular variables x_R stay constant, being $x_r' = 0, r \in R$. Then, the subsequent slow motion occurs in the regular variables on the manifold identified by $Z = Z_S^0$, and is described by the linear *reduced equation*:

$$\dot{x}_r = F_r(Z_S^0, B_{S'}, B_R) - \gamma_r x_r. \tag{2.5}$$

In accordance with singular perturbation theory, the solutions of the reduced and boundary layer equations, taken together, approximate the system dynamics for small q. Then, in the following we consider the full system in the limit $q \to 0$.

When both $S \neq \emptyset$ and $R \neq \emptyset$, a combination of fast and slow motion occurs: the fast motion moves along the switching variable direction followed by a slow motion that moves along the regular variable direction as illustrated in Fig. 2.1. As detailed in [14, 26], fast motion happens until a stable point Z_S^0, that satisfies the hypotheses of the Tikhonov-Wasow theorem, is reached. As the value of Z_S^0 indicates the point where the trajectory departs from the switching cross-section, we call it *exit point* of Δ. Similarly, we call *entrance point* the value of the initial condition of (2.4), as it indicates the point where the trajectory enters the switching cross section.

The location of the exit point, either on the boundary or in the interior of Δ depends on the parameter values $k_{il}, \gamma_i, \theta_{ij}$ in the boundary layer equations. According to whether the exit point is located, the system exhibits different behaviors. In the former case, where at least one component of Z_S^0 takes the integer value 0 or 1 on the domain boundary, the next motion occurs in an adjacent domain where the fast components become slow. In the latter case, internal Z_S^0, the regular motion *slides* along the manifold given by $Z = Z_S^0$, orthogonally to the switching thresholds of Δ, and towards the focal point $\Phi = (Z_S^0, x_R^*)$, whose regular components $x_r^* = F_r(Z_S^0)/\gamma_r,\ r \in R$, that depends on the parameters in (2.5), are assumed to never take threshold values, *i.e.*, $x_r^* \neq \theta_{rj}$ for all r and for all j. Such sliding motion occurs until it reaches either a stable point of (2.5), getting a system stable state, or a new threshold for any x_r, and enters a new domain (Fig. 2.1).

When either $S = N$ or $R = N$, only fast or slow motion occurs, respectively. The domains the trajectories move towards are given, in the former case, by the location of the exit points only; whereas, in the latter one, by the relative position of Φ with respect to the adjacent threshold values.

The localization of exit points, *i.e.*, the stationary solution of (2.4), is a crucial problem for the analysis of motion through a domain. Apart the stationary solutions $Z_s = 0$ and $Z_s = 1$ of (2.4) due to the factor D_s^0, in general, this problem is computationally hard to be solved, even for small networks, as it requires to solve a set of polynomial equations for which several solutions exist. But, under the assumption, biologically reasonable, that each transcription factor only regulates one gene at each threshold, or mathematically speaking that:

Assumption $\mathcal{A}$. Each variable Z_{ij} can appear at most in one equation in (2.1),

the set of polynomial equations are simplified to a set of linear equations with at most a single point-like solution if we disregard the rather unlikely situation that there could be infinitely many solutions. In other words, there is at most a single interior candidate Z_S^0 in each Δ [14].

2.2. Qualitative simulation of gene regulatory networks. When sufficient conditions that ensure the applicability of the singular perturbation method under

the above assumptions are satisfied, sound rules that determine the passage through any switching domain and, consequently, the sequence of traversed domains can be established [14]. Such rules underlie an automated analyzer/simulator that calculates the network dynamics that only depend on the model structure and are invariant for ranges of parameters [15]. It differs from a simulator that works under similar assumptions [13] in the way it (i) locally computes the transitions from domains characterized by multi-scale dynamics, and (ii) composes them to get all possible qualitatively distinct trajectories. This revised version results in an implemented algorithm significantly improved in terms of soundness, both local and global, efficiency, and characterization of the qualitative properties of the trajectories, e.g., cyclic and spiraling trajectories.

2.2.1. Local transitions between adjacent domains. The local analysis in the current domain $\Delta_a = \Delta(S_a, R_a, \theta_{S_a}, I_{R_a})$, mathematically rooted on the results in [26, 29] and definitively established in [14], aims at identifying all the possible candidate transitions to adjacent domains $\Delta_b = \Delta(S_b, R_b, \theta_{S_b}, I_{R_b})$, namely all possible candidate sets S_b, R_b, θ_{S_b}, I_{R_b}. The transition to a specific domain Δ_b is univocally determined by ranges on parameter values that make possible the motion from the entrance point to the exit point of the switching cross-section of Δ_a, and thus from the corresponding arrival point towards a specific departure point on the face of Δ_a at the boundary with Δ_b. More precisely, arrival/departure points are N-dimensional points on the boundaries of a domain at which a trajectory enters/leaves the domain. The switching variable coordinates are given by the entrance/exit point coordinates and the remaining R coordinates by the slow components of the motion of the regular variables in Δ_a. The parameter inequalities that state a one-to-one correspondence between an arrival point and a specific departure point result from both stability conditions and motion direction constraints.

By the exhaustive analysis of case equations given in [14], where the switching variables x_S are distinguished in x_V and x_U ($v \in V, u \in U$ and $S = V \cup U$) which were respectively regular and switching in the previous domain, the inequalities have specific structures that are determined by the model equations in Δ_a. Let k_{il} be the coefficients in the production term in the rate equation for x_i in Δ_a. The inequalities are either linear or bilinear in k_{il}, and take the following two forms only:

$$\begin{aligned} &\sum k_{il} \lesseqgtr \gamma_i \theta_{ij}, \\ &K_0 K_{uv} + K_u K_v \lesseqgtr \gamma_i \theta_{ij} K_{uv}, \end{aligned} \tag{2.6}$$

where K_0, K_{uv}, K_u, K_v are given by $\sum k_{il}$ associated with the constant terms, the coefficients of the terms $Z_u Z_v$, Z_u and Z_v of the equation for x_i, respectively.

2.2.2. Trajectory composition. Let us observe that for algorithmic purposes we number the domains in the phase space. Then, in accordance to our convenience we refer to a specific domain with either $\Delta(S, R, \theta_S, I_R)$ or D_i, where the value of i is easily calculated and depends on the number of variable thresholds and on the indexes in $\Delta(S, R, \theta_S, I_R)$, e.g., in Fig. 2.1 $\Delta(\{1, 2\}, \emptyset, \{\theta_{11}, \theta_{21}\}, \emptyset)$ is also labeled as D_7.

The algorithm performs an automated qualitative analysis of the model (2.1), and returns, in a single run, all the possible qualitative trajectories that start from an initial domain D_0 and with initial parameter space d^0 defined by parameter inequalities.

Through an iterative procedure, it constructs a tree rooted in D_0, where each node represents a domain, and each edge, labeled by parameter constraints, represents a

transition between two adjacent domains. At step k, from the current domain D_{i_k} it symbolically calculates the possible next transitions to $D_{i_{k+1}}$, denoted by $T_{i_k}^{i_{k+1}}$, and the inequalities on parameters, $d^{i_k,i_{k+1}}$, that must hold for the effective occurrence of the transition. The possible transitions together with their associated inequality constraints are given by a map of the arrival point in D_{i_k} to its proper departure point at the boundary with $D_{i_{k+1}}$ subject to $d^{i_k,i_{k+1}}$. As the map is obtained through exhaustive analysis of case equations [14], all and none but the transitions to the next adjacent domains are computed. Thus, the algorithm is locally complete and sound.

Each global trajectory $\mathcal{T}$ starting from a domain D_0 is calculated by properly composing in a sequence the local candidate transitions between adjacent domains, *i.e.*,

$$\begin{aligned}\mathcal{T} =< D_0, d^0 >, \cdots, < T_{i_{k-1}}^{i_k}, d^{i_{k-1},i_k} >, < T_{i_k}^{i_{k+1}}, d^{i_k,i_{k+1}} >, \cdots, \\ < T_{i_l}^{i_{\bar{l}}}, d^{i_l,i_{\bar{l}}} >, < D_{i_{\bar{l}}}, d^{i_{\bar{l}}} > .\end{aligned} \tag{2.7}$$

Each $T_{i_k}^{i_{k+1}}$ in the sequence is chained to its predecessor and successor transition, and the entire sequence of sets of inequalities $d^{i_k,i_{k+1}}$, given in the form (2.6), must be satisfied, *i.e.*, each $d^{i_k,i_{k+1}}$ must be compatible with all the others. In case the solvability of the whole sequence of inequalities is not verified, the generated trajectory is not globally sound, and then it is rejected. Thus, the resulting solution tree is globally complete and sound. The iteration process is finite, and the construction of each trajectory stops when either a stable fixed point is detected or a cycle is identified. In the former case, $i_l = i_{\bar{l}}$, a transition D_l to D_l itself is calculated and the correspondent inequality set $d^{l,l}$, for short d^l, is consistent with all the inequalities associated with the previous transitions in the sequence; in the latter one, a transition to a domain $D_{\bar{l}} = D_p$, where D_p is a domain previously visited in $\mathcal{T}$, is calculated, and its associated inequalities belong to the inequality set already calculated to reach D_p.

2.2.3. Example. To exemplify let us consider the following toy-example:

$$\begin{aligned}\dot{x}_1 =& k_{10} + k_{11}Z_{21} + k_{12}Z_{12} - \gamma_1 x_1, \\ \dot{x}_2 =& k_{21}Z_{11} - \gamma_2 x_2,\end{aligned} \tag{2.8}$$

and let us simulate it with initial condition in $D_5 = \Delta(\emptyset, \{1,2\}, \emptyset, \{2,0\})$, *i.e.*, $\theta_{12} < x_1 < \overline{x}_1 = max(x_1)$ and $0 < x_2 < \theta_{21}$, and inequality constraints $d^5 : \quad k_{10} > \gamma_1\theta_{12},\ k_{10}+k_{12} > \gamma_1\theta_{12},\ k_{10}+k_{11} < \gamma_1\theta_{11},\ k_{10}+k_{11} > 0, k_{21} > \gamma_2\theta_{21}$. By assumption, $\gamma_1,\ \gamma_2,\ \theta_{11},\ \theta_{12},\ \theta_{21} > 0$, and $\theta_{11} < \theta_{12}$.

With the given initial constraints the simulation produces 3 trajectories (Fig. 2.2). Although the example is very simple, it is interesting from the didactic point of view as it provides for different meaningful scenarios: trajectory 1 ends up in a stable fixed point in the regular domain D_{15}, trajectory 2 terminates its motion spiraling towards a stable point at threshold intersection in D_7 where the Jacobian has a specific structure and sign pattern, and trajectory 3, that goes back to the initial domain D_5, identifies a cyclic behavior not necessarily a periodic one. The trajectories are characterized by sequences of parameter inequalities $d^{i,j}$ that let the transition from D_i to D_j occur:

Trajectory 1 :
$d^5,\ d^{5,10},\ d^{10,15},\ d^{15,15}$;

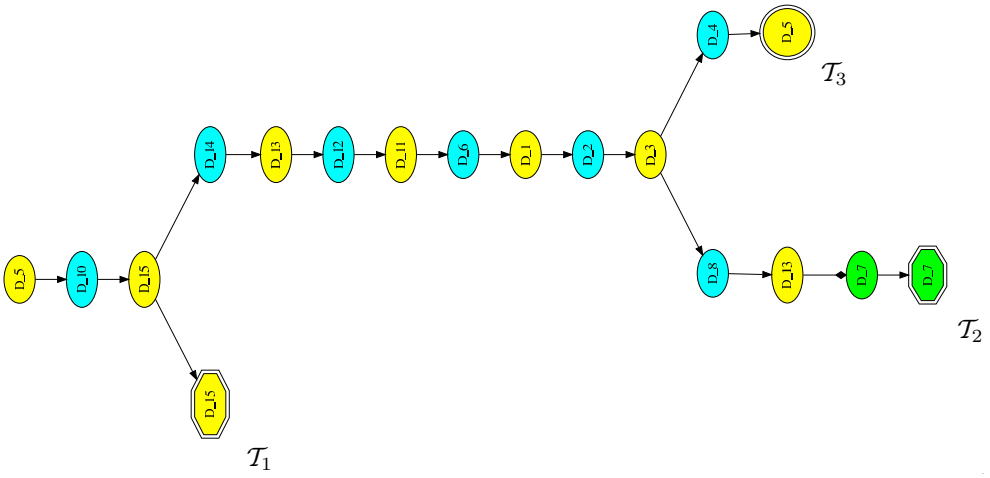

FIG. 2.2. *Solution tree of the simulation outcomes of the model in the example (2.8) with the given initial conditions. The simulation produces three different trajectories. Yellow circles denote regular domain whereas the blue and green ones denote switching domains characterized by both fast and slow motion, and fast motion only, respectively. The arrows denote the transition from one domain to another and a black filled diamond denotes that the motion spirals towards the domain. Octagonal final leaves denote domains with stable attractors whereas a double circle identifies a cycle.*

Trajectory 2 :
$d^5,\ d^{5,10},\ d^{10,15}, d^{15,14},\ d^{14,13},\ d^{13,12},\ d^{12,11},\ d^{11,6},\ d^{6,1},\ d^{1,2},\ d^{2,3},\ d^{3,8},\ d^{8,13},\ d^{13,7},\ d^{7,7}$;

Trajectory 3 :
$d^5,\ d^{5,10},\ d^{10,15},\ d^{15,14},\ d^{14,13},\ d^{13,12},\ d^{12,11},\ d^{11,6},\ d^{6,1},\ d^{1,2},\ d^{2,3},\ d^{3,4},\ d^{4,5}$.

The inequalities $d^{i,j}$ present in one or another of the trajectories are given in Table 2.1.

3. Assigning probabilities to trajectories. In a qualitative context, where the knowledge on the model parameters is given by initial order relations only, all possible trajectories are symbolically derived. The probability of the occurrence of each simulated trajectory can be calculated when knowledge on parameters is such that we can associate them with probability density functions. In the following, we propose a general method that, independent of the type of distribution set to each parameter, associates an occurrence probability with each branch in a given simulated solution tree, *i.e.*, with each possible system/network trajectory.

As already mentioned, the transitions in a solution tree depend on three sets of parameters, namely degradation rates, production rates and thresholds. Let Γ, K and Θ be the respective model parameter sets defined in accordance with the available stochastic knowledge, and let us denote by Ψ the stochastic parameter set given by $\Psi = K \cup \Gamma \cup \Theta$, with $|\Psi| = n_c$. The uncertainty of parameter values $\psi_i \in \Psi$ is expressed by *a priori* independent density functions that are chosen in accordance with the available knowledge on the network: the more complete is the knowledge of a parameter value the lower should be the variance of its distribution. In general, the physics of the system suggests continuous density functions, whose shapes can be either given in accordance with a standardized form (e.g., normal densities, gamma

Inequality Constraints	
T_i^j	$d^{i,j}$
T_1^2	$k_{10} > \gamma_1\theta_{11}$
T_2^3	$k_{10} > \gamma_1\theta_{11}$
T_3^4	$k_{10} > \gamma_1\theta_{12}$
T_3^8	$k_{21} > \gamma_2\theta_{21}$
T_4^5	$k_{10} + k_{12} > \gamma_1\theta_{12}$
T_5^{10}	$k_{21} > \gamma_2\theta_{21}$
T_6^1	$\gamma_2\theta_{21} > 0$
T_7^7	$\gamma_2\theta_{21} > 0;\ k_{21} > \gamma_2\theta_{21};\ k_{10} > \gamma_1\theta_{11};\ k_{21} > 0;\ k_{11} < 0$
T_8^{13}	$k_{21} > \gamma_2\theta_{21}$
T_{10}^{15}	$k_{21} > \gamma_2\theta_{21}$
T_{11}^6	$\gamma_2\theta_{21} > 0$
T_{12}^{11}	$k_{10} + k_{11} < \gamma_1\theta_{11}$
T_{13}^7	$\gamma_2\theta_{21} > 0;\ \gamma_1\theta_{11} > 0$
T_{13}^{12}	$k_{10} + k_{11} < \gamma_1\theta_{11}$
T_{14}^{13}	$k_{10} + k_{11} + k_{12} < \gamma_1\theta_{12};\ k_{10} + k_{11} < \gamma_1\theta_{12}$
T_{15}^{14}	$k_{10} + k_{11} + k_{12} < \gamma_1\theta_{12}$
T_{15}^{15}	$k_{10} + k_{11} + k_{12} > \gamma_1\theta_{12};\ k_{10} + k_{11} + k_{12} < \gamma_1\overline{x}_1;\ k_{21} > \gamma_2\theta_{21};\ k_{21} < \gamma_2\overline{x}_2$

TABLE 2.1

Parameter inequalities that hold for the occurrence of a transition T_i^j from a domain D_i to the next one D_j.

densities, *etc.*) or constructed *ad hoc*.

The choice of density functions must fulfill the modeling assumptions that, in case of very incomplete knowledge, represent the only certain constraints on parameters. In such a case, uniform distributions with large supports suitably represent modeling constraints on parameter values, only.

If available knowledge is such that distributions can be concentrated around a value, suggestions for possible suitable densities are given below:

- Degradation rate parameters (γ_i): they are positive by assumption, and a unimodal distribution is usually an appropriate choice. The most common unimodal distribution with positive support is the *Gamma* density ($f_i^{priori}(\gamma_i) \sim Gamma(\alpha_i, \beta_i)$) where the parameters α_i and β_i have to be chosen so that $f_i^{priori}(0) = 0$.
- Production rate parameters (k_{il}): they can assume both positive or negative values. If the sign is explicitly given or implicitly carried by the initial conditions, *Gamma* distributions are appropriate also in this case: $f_i^{priori}(k_{il}) \sim Gamma(\alpha_i, \beta_i)$ if $k_{il} > 0$, and $f_i^{priori}(-k_{il}) \sim Gamma(\alpha_i, \beta_i)$ if $k_{il} < 0$. Otherwise, a bimodal distribution is suggested, with a null probability of $k_{il} = 0$. The combination of two equal *Gamma* distributions is the most simple solution: the absolute value follows a *Gamma* distribution ($f_i^{priori}(|k_{il}|) \sim Gamma(\alpha_i, \beta_i)$) and the sign of k_{il} follows a Bernoulli distribution with parameter 0.5.
- Threshold parameters (θ_{ij}): they are always assumed to be positive. Moreover, the thresholds $\theta_{ij},\ j = 1, \ldots, m_i$ associated with each state variable x_i are ordered and well-separated. As a consequence, parameters θs have to take values in a limited range, between a minimum and a maximum value,

and have to respect threshold ordering and domain disjunction. Ordering and disjunction of supports is properly represented by uniform distributions ($f_i^{priori}(\theta_{ij}) \sim U(a_{ij}, b_{ij})$) with $b_{ij} < a_{i\ j+1}$. Moreover, their supports (a_{ij}, b_{ij}) can be narrow when threshold parameters can be identified by gene expression profiles [6].

Whenever the knowledge on parameters is good enough to limit their ranges of variability $[\alpha, \beta]$ and to concentrate their values around a peak μ, truncated Gaussian distributions $\mathcal{TN}\left(\mu, \sigma^2, \alpha, \beta\right)$ provide suitable alternatives. The analytical expression of such density is as follows:

$$f_i^{priori}(\psi_i) = \frac{e^{-\frac{1}{2\sigma^2}(\psi_i - \mu)^2}}{\sqrt{2\pi\sigma^2}\left[\phi\left(\frac{\beta-\mu}{\sigma}\right) - \phi\left(\frac{\alpha-\mu}{\sigma}\right)\right]} 1_{(\alpha,\beta)}$$

where ϕ is the cumulative density function of the standard normal distribution $\mathcal{N}(0,1)$. Let us remark that, since the distribution is truncated, μ and σ^2 do not represent any more the expected value and variance of ψ_i.

The set Ψ is characterized by a continuous joint probability density function $f_0(\Psi)$ with support in $\mathcal{V}_0$, where $\mathcal{V}_0 \subseteq \mathbb{R}^{n_c}$ is the range of variability defined by the initial parameter inequality constraints (*i.e.*, $\mathcal{V}_0$ includes all and only values of Ψ that satisfy the initial inequality system). Starting from the *a priori* densities, $f_0(\Psi)$ results from restricting the support of all densities $f_i^{priori}(\psi_i)$ to $\mathcal{V}_0$. As the *a priori* marginal densities are assumed to be independent and the joint *a priori* density is given by their product, $f_0(\Psi)$ is:

$$f_0(\Psi) = \begin{cases} \frac{\prod_{i=1}^{n_c} f_i^{priori}(\psi_i)}{\int_{\mathcal{V}_0}\left[\prod_{i=1}^{n_c} f_i^{priori}(\psi_i)\right] d\psi_1 \ldots d\psi_{n_c}} & \Psi \in \mathcal{V}_0 \\ 0 \qquad\qquad elsewhere \end{cases} \tag{3.1}$$

We underline that, in our approach, even if the parameters ψ_i are assumed to be independent in the *a priori* densities, in $f_0(\Psi)$ they are not independent any more due to the shape of $\mathcal{V}_0$ itself. In fact, the independence between parameters ψ_i is not maintained after the support restriction because $\mathcal{V}_0$ is in general not simple (according to the definition of simple regions for multiple integrals) with respect to the components ψ_i. As a consequence, $f_0(\Psi)$ cannot be factorized into the product of its marginal densities.

As defined in (2.7), a trajectory $\mathcal{T}$ consists of a chain of subsequent transitions T_i^j which start from an initial domain and end in a final domain that either contains an attractor or identifies a cycle. The occurrence of each transition T_i^j in $\mathcal{T}$ implies that the systems of inequalities $d^{i,j}$ of all previous transitions in the same $\mathcal{T}$ are satisfied. As a consequence, given two subsequent transitions T_a^b and T_b^c, and the ranges of variability $\mathcal{V}_a$ and $\mathcal{V}_b$ in which inequality systems $d^{a,b}$ and $d^{b,c}$ are evaluated, respectively, it follows that $\mathcal{V}_c \subseteq \mathcal{V}_b \subseteq \mathcal{V}_a \subseteq \mathcal{V}_0$. Secondary to the reduction of its support, the joint density function is cut with a consequent change of its shape. Given a range $\mathcal{V}_i$, let us denote by $f_i(\Psi)$ the joint density function with support in $\mathcal{V}_i$.

3.1. Probability of a local transition. As already mentioned, an admissible transition T_a^b between domain Δ_a and domain Δ_b is associated with a system $d^{a,b}(\Psi)$ of m inequalities, where each inequality $d_j^{a,b}(\Psi) > 0$ has a linear or bilinear structure as in (2.6).

In the stochastic setting, unlike the deterministic case where each inequality is either *verified* or *not verified*, the solution of each inequality is given in terms of

the probability to be satisfied. This is the expected value of a Bernoulli stochastic variable. Similarly, the solution of the system $d^{a,b}(\Psi)$ is the expected value of another Bernoulli stochastic variable, which represents the probability $P[d^{a,b}]$ that the system is satisfied.

The Bernoulli variable of the system can be expressed as $\prod_{j=1}^{m} 1_{d_j^{a,b}(\Psi)}$, where 1_h is the indicator function equal to 1 if $h > 0$ and 0 elsewhere. Thus:

$$P[d^{a,b}] = E\left[\prod_{j=1}^{m} 1_{d_j^{a,b}(\Psi)}\right] = \int_{\mathcal{V}_a} \left[\prod_{j=1}^{m} 1_{d_j^{a,b}(\Psi)}\right] f_a(\Psi)\, d\psi_1 \ldots d\psi_{n_c}, \tag{3.2}$$

We remark that $P[d^{a,b}]$ is conditional because it requires that the state variables have previously reached domain Δ_a from which the transition under analysis occurs. The conditional term could be explicited by adopting the notation $P\left[d^{a,b}|\Delta_a\right]$, even if this is neglected in the following for the sake of simplicity.

In general, the m inequalities $d_j^{a,b}(\Psi)$ are not independent, because variables ψ_i may appear in more than one $d_j^{a,b}(\Psi)$. Hence, the probability $P[d^{a,b}]$ cannot be factorized into the probabilities of the single inequalities and, then, the inequalities cannot be studied separately.

The probability $P[d^{a,b}]$ is assumed to be the probability of the transition $P[T_a^b]$ when one single path is admissible from Δ_a. But, as highlighted in Fig. 2.2, multiple paths can branch off from a domain. For the sake of clarity, we start the analysis considering the case of two possible transitions from the same domain and, then, we extend the discussion to any number of possible transitions.

Let us consider two transitions from domain Δ_a to domains Δ_b and Δ_c, constrained by the inequality systems $d^{a,b}$ and $d^{a,c}$, respectively. The probabilities of the inequality systems $d^{a,b}$ and $d^{a,c}$ are calculated according to (3.2):

$$P[d^{a,b}] = \int_{\mathcal{V}_a} \left[\prod_{j=1}^{m} 1_{d_j^{a,b}(\Psi)}\right] f_a(\Psi)\, d\psi_1 \ldots d\psi_{n_c};$$

$$P[d^{a,c}] = \int_{\mathcal{V}_a} \left[\prod_{j=1}^{m} 1_{d_j^{a,c}(\Psi)}\right] f_a(\Psi)\, d\psi_1 \ldots d\psi_{n_c}.$$

Moreover, the probability $P[d^{a,b\wedge c}]$ that the systems $d^{a,b}$ and $d^{a,c}$ are both satisfied is still determined according to (3.2), after enclosing the two inequality systems $d^{a,b}$ and $d^{a,c}$ in a single system $d^{a,b\wedge c}$:

$$P[d^{a,b\wedge c}] = \int_{\mathcal{V}_a} \left[\prod_{j=1}^{m} 1_{d_j^{a,b\wedge c}(\Psi)}\right] f_a(\Psi)\, d\psi_1 \ldots d\psi_{n_c}.$$

Due to soundness and completeness of the algorithm, at least one or the other of the systems $d^{a,b}$ and $d^{a,c}$ is verified in each point of $\mathcal{V}_a$, and two possible situations can occur:

Case 1: the two inequality systems $d^{a,b}$ and $d^{a,c}$ are mutually alternative, *i.e.*, they work on the same parameters ψ_i (all the set Ψ or a part of it) with mutually

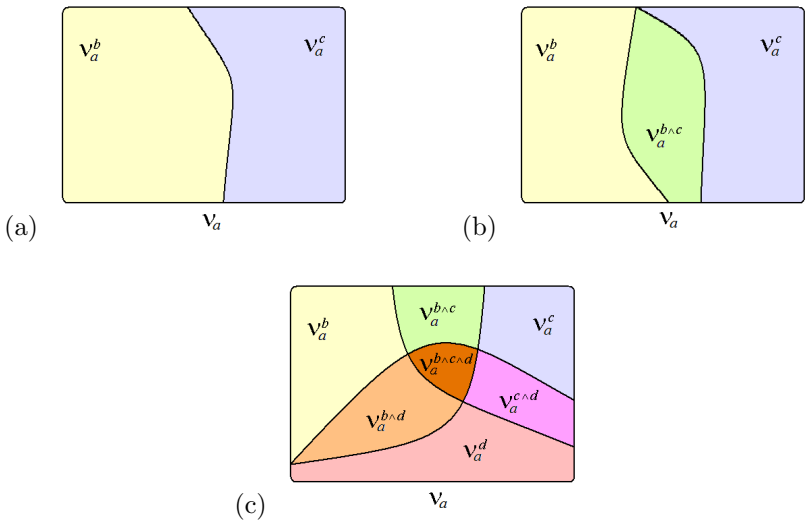

FIG. 3.1. *Splitting of $\mathcal{V}_a$ in different cases: (a) two mutually alternative inequality systems $d^{a,b}$ and $d^{a,c}$; (b) two not mutually alternative inequality systems $d^{a,b}$ and $d^{a,c}$; (c) three not mutually alternative inequality systems $d^{a,b}$, $d^{a,c}$ and $d^{a,d}$.*

alternative inequalities. If one of the two systems is satisfied for a specific set of values assigned to Ψ, the other system is necessarily unsatisfied for the same set. This means that the range of variability $\mathcal{V}_a$ is partitioned into two parts $\mathcal{V}_a^b$ and $\mathcal{V}_a^c$. Values of $\Psi \in \mathcal{V}_a^b$ allow transition T_a^b and values of $\Psi \in \mathcal{V}_a^c$ allow transition T_a^c (Fig. 3.1a).
Thus, $P[d^{a,b\wedge c}] = 0$, and the probabilities of the transitions $P[T_a^b]$ and $P[T_a^c]$ are straightforward defined:

$$P[T_a^b] := P[d^{a,b}]; \qquad P[T_a^c] := P[d^{a,c}].$$

Case 2: the two inequality systems $d^{a,b}$ and $d^{a,c}$ are not mutually alternative. This means that they work on different parameters ψ_i or, alternatively, on the same parameters but the systems are not mutually alternative. In this case, for certain values assigned to Ψ, if one of the two systems is satisfied also the other is satisfied. Hence, $P[d^{a,b\wedge c}] > 0$. In this case, $\mathcal{V}_a^b$ and $\mathcal{V}_a^c$ do not represent a partition of $\mathcal{V}_a$ because they have a non-empty intersection, denoted with $\mathcal{V}_a^{b\wedge c}$, in which both the inequality systems are satisfied (Fig. 3.1b). Indeed, we have:

$$\begin{aligned} &\mathcal{V}_a = (\mathcal{V}_a^b \setminus \mathcal{V}_a^{b\wedge c}) \cup (\mathcal{V}_a^c \setminus \mathcal{V}_a^{b\wedge c}) \cup \mathcal{V}_a^{b\wedge c}; \\ &(\mathcal{V}_a^b \setminus \mathcal{V}_a^{b\wedge c}) \cap (\mathcal{V}_a^c \setminus \mathcal{V}_a^{b\wedge c}) = \emptyset. \end{aligned} \tag{3.3}$$

Due to (3.3), the probabilities of the inequality systems are related as follows:

$$\begin{aligned} 1 &= \big(P[d^{a,b}] - P[d^{a,b\wedge c}]\big) + \big(P[d^{a,c}] - P[d^{a,b\wedge c}]\big) + P[d^{a,b\wedge c}] = \\ &= \left(P[d^{a,b}] - \frac{1}{2}P[d^{a,b\wedge c}]\right) + \left(P[d^{a,c}] - \frac{1}{2}P[d^{a,b\wedge c}]\right). \end{aligned}$$

As $P[d^{a,b\wedge c}] > 0$ the estimation of the transition probabilities is given within a range. More precisely, $P[T_a^b] \in \big[P[d^{a,b}] - P[d^{a,b\wedge c}],\ P[d^{a,b}]\big]$ and $P[T_a^c] \in$

$\left[P[d^{a,c}] - P[d^{a,b\wedge c}],\ P[d^{a,c}]\right]$. To equally account for $P[d^{a,b\wedge c}]$ between the transitions, we associate these ranges with uniform distributions and define $P[T_a^b]$ and $P[T_a^c]$ as the expected values of these distributions:

$$\begin{aligned} P[T_a^b] &:= P[d^{a,b}] - \frac{1}{2}P[d^{a,b\wedge c}]; \\ P[T_a^c] &:= P[d^{a,c}] - \frac{1}{2}P[d^{a,b\wedge c}]. \end{aligned} \tag{3.4}$$

Obviously, this definition obeys $P\left[T_a^b\right] + P\left[T_a^c\right] = 1$.

In the presence of more than two not mutually alternative transitions, all of the resulting divisions of $\mathcal{V}_a$ have to be evaluated.

As for three possible transitions T_a^b, T_a^c and T_a^d from domain Δ_a to domains Δ_b, Δ_c and Δ_d, $\mathcal{V}_a$ is divided in three overlapped parts $\mathcal{V}_a^b$, $\mathcal{V}_a^c$ and $\mathcal{V}_a^d$. Different intersections appear: three intersections $\mathcal{V}_a^{b\wedge c}$, $\mathcal{V}_a^{b\wedge d}$ and $\mathcal{V}_a^{c\wedge d}$ between two parts, and one intersection $\mathcal{V}_a^{b\wedge c\wedge d}$ between all the three parts (Fig. 3.1c). Then, we have:

$$\begin{aligned} \mathcal{V}_a = &(\mathcal{V}_a^b \setminus \mathcal{V}_a^{b\wedge c} \cup \mathcal{V}_a^{b\wedge c\wedge d} \setminus \mathcal{V}_a^{b\wedge d}) \cup (\mathcal{V}_a^c \setminus \mathcal{V}_a^{b\wedge c} \cup \mathcal{V}_a^{b\wedge c\wedge d} \setminus \mathcal{V}_a^{c\wedge d}) \cup \\ &\cup (\mathcal{V}_a^d \setminus \mathcal{V}_a^{b\wedge d} \cup \mathcal{V}_a^{b\wedge c\wedge d} \setminus \mathcal{V}_a^{c\wedge d}) \cup (\mathcal{V}_a^{b\wedge c} \setminus \mathcal{V}_a^{b\wedge c\wedge d}) \cup (\mathcal{V}_a^{b\wedge d} \setminus \mathcal{V}_a^{b\wedge c\wedge d}) \cup \\ &\cup (\mathcal{V}_a^{c\wedge d} \setminus \mathcal{V}_a^{b\wedge c\wedge d}) \cup (\mathcal{V}_a^{b\wedge c\wedge d}); \end{aligned} \tag{3.5}$$

where the subsets in parentheses partition $\mathcal{V}_a$ because they have empty intersections. As $\mathcal{V}_a^{b\wedge c\wedge d}$ is included in all three $\mathcal{V}_a^{b\wedge c}$, $\mathcal{V}_a^{b\wedge d}$ and $\mathcal{V}_a^{c\wedge d}$, the term "$\cup\mathcal{V}_a^{b\wedge c\wedge d}$" in the first three parentheses compensates for the double subtraction.

Similar to the previous case, due to (3.5) and the empty intersections, the probabilities of the systems are related as follows:

$$\begin{aligned} 1 = &\left(P[d^{a,b}] - P[d^{a,b\wedge c}] + P[d^{a,b\wedge c\wedge d}] - P[d^{a,b\wedge d}]\right) + \\ &+ \left(P[d^{a,c}] - P[d^{a,b\wedge c}] + P[d^{a,b\wedge c\wedge d}] - P[d^{a,c\wedge d}]\right) + \\ &+ \left(P[d^{a,d}] - P[d^{a,b\wedge d}] + P[d^{a,b\wedge c\wedge d}] - P[d^{a,c\wedge d}]\right) + \\ &+ \left(P[d^{a,b\wedge c}] - P[d^{a,b\wedge c\wedge d}]\right) + \left(P[d^{a,b\wedge d}] - P[d^{a,b\wedge c\wedge d}]\right) + \\ &+ \left(P[d^{a,c\wedge d}] - P[d^{a,b\wedge c\wedge d}]\right) + P[d^{a,b\wedge c\wedge d}] = \\ &= \left(P[d^{a,b}] - \frac{1}{2}P[d^{a,b\wedge c}] - \frac{1}{2}P[d^{a,b\wedge d}] + \frac{1}{3}P[d^{a,b\wedge c\wedge d}]\right) + \\ &+ \left(P[d^{a,c}] - \frac{1}{2}P[d^{a,b\wedge c}] - \frac{1}{2}P[d^{a,c\wedge d}] + \frac{1}{3}P[d^{a,b\wedge c\wedge d}]\right) + \\ &+ \left(P[d^{a,d}] - \frac{1}{2}P[d^{a,b\wedge d}] - \frac{1}{2}P[d^{a,c\wedge d}] + \frac{1}{3}P[d^{a,b\wedge c\wedge d}]\right). \end{aligned}$$

We define $P[T_a^b]$, $P[T_a^c]$ and $P[T_a^d]$ so that $P[T_a^b] + P[T_a^c] + P[T_a^d] = 1$ and they equally account for the intersections:

$$\begin{aligned} P[T_a^b] &:= P[d^{a,b}] - \frac{1}{2}P[d^{a,b\wedge c}] - \frac{1}{2}P[d^{a,b\wedge d}] + \frac{1}{3}P[d^{a,b\wedge c\wedge d}]; \\ P[T_a^c] &:= P[d^{a,c}] - \frac{1}{2}P[d^{a,b\wedge c}] - \frac{1}{2}P[d^{a,c\wedge d}] + \frac{1}{3}P[d^{a,b\wedge c\wedge d}]; \\ P[T_a^d] &:= P[d^{a,d}] - \frac{1}{2}P[d^{a,b\wedge d}] - \frac{1}{2}P[d^{a,c\wedge d}] + \frac{1}{3}P[d^{a,b\wedge c\wedge d}]. \end{aligned}$$

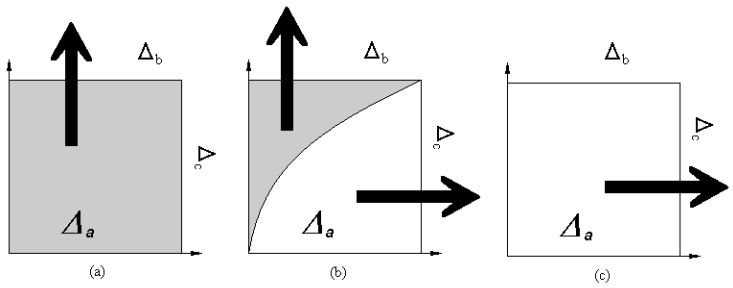

FIG. 3.2. *Possible transitions from domain Δ_a. Values of parameter set in: (a) $\mathcal{V}_a^b \setminus \mathcal{V}_a^{b\wedge c}$ or $\mathcal{V}_a^b$ (for mutually alternative transitions); (b) $\mathcal{V}_a^{b\wedge c}$ for which the actual transition depends on the specific coordinates of the initial state within Δ_a; (c) $\mathcal{V}_a^c \setminus \mathcal{V}_a^{b\wedge c}$ or $\mathcal{V}_a^c$ (for mutually alternative transitions).*

In the general case, with more than three admissible transitions from domain Δ_a, transition probabilities $P[T_a^i]$ to each domain Δ_i are similarly defined.

Remark. In qualitative simulation, two or more transitions are all possible from a given domain Δ_a because both the initial state and the parameters are not given a specific value. As for the state, we recall that the qualitative value abstracts the value of coordinates in the whole domain. With reference to two transitions, in *Case* 1, where mutually alternative systems of inequalities characterize the transitions and $P[d^{a,b\wedge c}] = 0$, only either one or the other transition occurs for all values of parameter set in $\mathcal{V}_a$, independently of the specific coordinates of the initial state in the domain. As for *Case* 2, where $P[d^{a,b\wedge c}] > 0$, only either one or the other transition occurs for parameter values either in $\mathcal{V}_a^b \setminus \mathcal{V}_a^{b\wedge c}$ or $\mathcal{V}_a^c \setminus \mathcal{V}_a^{b\wedge c}$, independently of the specific coordinates of the initial state in the domain, as in the previous case. On the contrary, both transitions are allowed for values of parameter set in $\mathcal{V}_a^{b\wedge c}$: this holds because the actual occurrence of one or the other depends on the specific initial state value within Δ_a (Fig. 3.2).

3.2. Probability of a trajectory. The probability of occurrence of a trajectory $\mathcal{T}$ is given by the composition of the probabilities of the transitions in $\mathcal{T}$.

Let $\mathcal{T}_k$ be a sub-trajectory of $\mathcal{T}$ made up of its first k transitions, and $T_{i_{k-1}}^{i_k}$ the last transition in $\mathcal{T}_k$. It holds:

$$P[\mathcal{T}_k] = P[T_{i_{k-1}}^{i_k}] \cdot P[\mathcal{T}_{k-1}] = P[T_{i_{k-1}}^{i_k}] \cdot P[T_{i_{k-2}}^{i_{k-1}}] \cdot P[\mathcal{T}_{k-2}] = P[\mathcal{T}_0] \cdot \prod_{l=1}^{k} P[T_{i_{l-1}}^{i_l}],$$

where $\mathcal{T}_0$ denotes the sub-trajectory given by the initial domain only, and $P[\mathcal{T}_0]$ gives the probability that the initial inequalities are satisfied in $\mathcal{V}_0$. Thus, $P[\mathcal{T}_0] = 1$ in $\mathcal{V}_0$. We observe that $P[\mathcal{T}_k]$ is a chain of conditional probabilities, and not the product of independent probabilities, because each $P[T_{i_{k-1}}^{i_k}]$ is a conditional probability which requires the arrival in domain $D_{i_{k-1}}$. Then, the probability of the entire trajectory $\mathcal{T}$, including $\bar{k}$ transitions, is given by:

$$P[\mathcal{T}] = \prod_{l=1}^{\bar{k}} P[T_{i_{l-1}}^{i_l}].$$

Each conditional probability $P[T_{i_{k-1}}^{i_k}]$ is given in accordance with the definitions in the previous section. The range of variability $\mathcal{V}_{i_{k-1}}$ and the probability density function $f_{i_{k-1}}(\Psi)$ required for the computation in (3.2) derive from the sub-trajectory $\mathcal{T}_{k-1}$. The range is:

$$\mathcal{V}_{i_{k-1}} = \mathcal{V}_0 \cap \left\{ \Psi \in \mathbb{R}^{n_c} : \prod_{j=1}^{q} 1_{d_j^{(k-1)}(\Psi)} = 1 \right\} \tag{3.6}$$

where $d_j^{(k-1)}(\Psi) > 0$ are the q inequalities associated with $\mathcal{T}_{k-1}$.

The function $f_{i_{k-1}}(\Psi)$ is then obtained by reducing the support of $f_0(\Psi)$ to $\mathcal{V}_{i_{k-1}}$, or by directly reducing the support of the *a priori* joint density (*i.e.*, $\prod_{j=1}^{n_c} f_j^{priori}(\psi_j)$) to $\mathcal{V}_{i_{k-1}}$ as follows:

$$f_{i_{k-1}}(\Psi) = \begin{cases} \frac{\prod_{j=1}^{n_c} f_j^{priori}(\psi_j)}{\int_{\mathcal{V}_{i_{k-1}}} \left[\prod_{j=1}^{n_c} f_j^{priori}(\psi_j)\right] d\psi_1 \ldots d\psi_{n_c}} & \Psi \in \mathcal{V}_{i_{k-1}} \\ 0 & \textit{elsewhere} \end{cases} \tag{3.7}$$

In general, the integrals over $\mathcal{V}_{i_{k-1}}$ in (3.2) and (3.7) have not a closed-form analytical solution because $\mathcal{V}_{i_{k-1}}$ is usually not simple (according to the definition of simple regions for multiple integrals) with respect to the components ψ_j. Hence, a numerical solution is required. To this aim, we adopt the Monte Carlo integration approach detailed in the Appendix.

The definitions given above apply to all of the three types of trajectories generated by the simulation algorithm; namely, trajectories that reach a stable fixed point, either directly or spiraling around it, and trajectories that move in a cycle. However, spiraling and cycling trajectories require further discussion.

3.2.1. Spiraling trajectories. In this case, $\mathcal{T}$ spirals in a gradual progression towards an asymptotically stable point x_{ssp} in a domain D_f, called *hub*, where all variables are at threshold intersection. This implies that a sequence of traversed domains is repeated until the trajectory enters D_f and the spiral stable point x_{ssp} is reached. In the limit, at x_{ssp}, the Jacobian of the model has a specific structure and sign pattern [14].

From a computational point of view, the repetition of the same sequence of traversed domains should be avoided. Thus, as soon as a cycle around domains adjacent to a hub is detected, *i.e.*, a transition gets a domain D_k that coincides with a domain D_i previously visited in the sub-trajectory, the algorithm ascertains the presence of a possible spiral stable point in the hub by checking the structure and sign pattern of the Jacobian. If a spiraling behavior is recognized, in the solution tree the transitions in the next cycles from D_k to the final hub domain D_f are collapsed into a single transition from D_k to D_f. Let us remark that transitions in a spiral are uniquely determined with probability equal to 1. Thus, the probability associated with the entire trajectory $P[\mathcal{T}]$ is not actually affected by the spiraling around D_f, and can be computed taking into account the transitions which are reported in the solution tree, only.

3.2.2. Cycling trajectories. In the case a cycle is identified but a spiraling trajectory is not detected, the same transitions can be repeated an infinite number of times. As in the spiraling case, the solution tree does not contain the repeated transitions but terminates in the domain D_k that identifies the cycle (see Fig.2.2).

At each repetition of the cycle, both uniquely determined and mutually alternative transitions have probability equal to 1 to remain in the cycle. Hence, if all of the transitions in the cycle are as above, the next cycles have probability to be repeated equal to 1, and $P[\mathcal{T}]$ is not affected by the successive repetitions of the cycle, but it is determined by the probabilities of the transitions actually present in the solution tree, only.

In the presence of not mutually alternative transitions that branch from a domain in the cycle (e.g., the transitions from D_3 in Fig. 2.2), at each repetition, the probability to follow the cycle accounts for the probability to escape to domains other than those in the cycle. Without loss of generality, let us consider a domain D_{br} in the cycle from which two not mutually alternative transitions branch. We denote the transition that moves along the cycle by T_{br}^{cyc}, and the one that escapes from the cycle by T_{br}^{esc}. At each next cycle repetition, $\mathcal{V}_{br} \equiv \mathcal{V}_{br}^{cyc}$, and consequently $\mathcal{V}_{br}^{esc} \setminus \mathcal{V}_{br}^{cyc \wedge esc} = \emptyset$. The trajectory goes along the cycle an infinite number of times for parameter values in $\mathcal{V}_{br}^{cyc} \setminus \mathcal{V}_{br}^{cyc \wedge esc}$ but it could escape from the cycle for parameter values in $\mathcal{V}_{br}^{cyc \wedge esc}$. In the former case, $P[\mathcal{T}]$ is still not affected by the successive repetitions of the cycle and computed by considering the transitions in the solution tree, only. In the latter one, $P[\mathcal{T}]$ is still as above if cycle permanence is guaranteed; otherwise $P[\mathcal{T}]$ is upper bounded by the probability of its sub-trajectory $\mathcal{T}^*$ that starts from D_0 and terminates in D_k as calculated from the solution tree.

3.3. Back to the example. To illustrate how the proposed stochastic approach works, let us consider the toy-example in subsect. 2.2.3.

As shown in Fig. 2.2, the simulation of model (2.8) from the initial domain D_5 with the given initial parameter inequalities produces three trajectories. Two transitions subject to mutually alternative inequality systems branch from domain D_{15}. The transition T_{15}^{15} occurs when parameter inequalities lead the motion to a stable point in D_{15}, and then identifies the final leaf of the trajectory $\mathcal{T}_1$. The other transition T_{15}^{14} leads to a sub-trajectory that branches towards D_8 and D_4 with parameter inequalities d^{D_3,D_8} and d^{D_3,D_4}, respectively, when D_3 is reached. These two inequality systems, that govern the transitions T_3^8 and T_3^4, are not mutually alternative. Moreover, they are both always verified in the range $\mathcal{V}_{D_3}$ as they replicate initial parameter inequalities. Thus, $P\left[d^{D_3,D_8}\right] = P\left[d^{D_3,D_4}\right] = P\left[d^{D_3,D_8 \wedge D_4}\right] = 1$ always occurs independently of the assumed parameter densities and, in accordance with (3.4), we assign $P\left[T_3^8\right] = P\left[T_3^4\right] = 0.5$. In both branches from D_3, the motion continues to the final leaves of $\mathcal{T}_2$ and $\mathcal{T}_3$ without further ramifications: the branch towards D_4 goes back to the initial domain D_5, where a cycle is detected, and that one towards D_8 continues to D_{13} where a spiralling motion to a stable point in D_7 is recognized.

Due to the presence of not mutual alternative transitions from D_3, the actual value of $P[\mathcal{T}_3]$ is affected by the successive repetitions of the cycle and, in absence of periodic solutions, the probability of remaining in the cycle tends to zero after many passages. This holds for each parameter value as $P\left[d^{D_3,D_8 \wedge D_4}\right] = 1$. As a consequence, the solution tree includes only the sub-trajectories $\mathcal{T}_2^*$ and $\mathcal{T}_3^*$ of $\mathcal{T}_2$ and $\mathcal{T}_3$, respectively, that start from the initial domain D_5 and end in the final leaf. The computed value $P[\mathcal{T}_3^*]$ is an upper bound for the actual value of the occurrence probability of $\mathcal{T}_3$, whereas the computed value of $P[\mathcal{T}_2^*]$ is a lower bound for $P[\mathcal{T}_2]$. In addition, due to the structure of the tree, it holds $P[\mathcal{T}_2^*] = P[\mathcal{T}_3^*] = \frac{1}{2}(1 - P[\mathcal{T}_1])$, and $P[\mathcal{T}_2] + P[\mathcal{T}_3] = 1 - P[\mathcal{T}_1]$.

The values of the trajectory probabilities depend on the densities of parameters that appear in the inequalities, namely k_{10}, k_{11}, k_{12}, k_{21}, γ_1, γ_2, θ_{11}, θ_{12} and θ_{21}. To

	Case 1	Case 2	Case 3	Case 4
k_{10}	$\mathcal{N}(7,4)$	$\mathcal{N}(16,4)$	$\mathcal{N}(5,4)$	$\mathcal{N}(3,4)$
k_{11}	$\mathcal{N}(-4,4)$	$\mathcal{N}(-11,4)$	$\mathcal{N}(0,4)$	$\mathcal{N}(0,4)$
k_{12}	$\mathcal{N}(-4,4)$	$\mathcal{N}(3,4)$	$\mathcal{N}(1,4)$	$\mathcal{N}(4,4)$
k_{21}	$\mathcal{N}(10,4)$	$\mathcal{N}(12,4)$	$\mathcal{N}(12,4)$	$\mathcal{N}(10,4)$
γ_1	$Gamma(3,1)$	$Gamma(3,1)$	$Gamma(3,1)$	$Gamma(3,1)$
γ_2	$Gamma(10,1)$	$Gamma(10,1)$	$Gamma(10,1)$	$Gamma(10,1)$
θ_{11}	$\mathcal{U}(0.8,1.2)$	$\mathcal{U}(0.8,1.2)$	$\mathcal{U}(0.8,1.2)$	$\mathcal{U}(0.8,1.2)$
θ_{12}	$\mathcal{U}(1.8,2.2)$	$\mathcal{U}(1.8,2.2)$	$\mathcal{U}(1.8,2.2)$	$\mathcal{U}(1.8,2.2)$
θ_{21}	$\mathcal{U}(0.8,1.2)$	$\mathcal{U}(0.8,1.2)$	$\mathcal{U}(0.8,1.2)$	$\mathcal{U}(0.8,1.2)$
$P[\mathcal{T}_1]$	0.004	0.212	0.334	0.830
$P[\mathcal{T}_2^*]$	0.498	0.395	0.339	0.086
$P[\mathcal{T}_3^*]$	0.498	0.395	0.339	0.086

TABLE 3.1

Probabilities of the occurrence of the simulated dynamics for the toy-example in subsect. 2.2.3.for different choices of parameter distributions. The results are obtained by exploiting the standard Monte Carlo integration, with 10^6 generated samples for each probability. All confidence intervals of the estimated probabilities are below 0.001. We remark that $\mathcal{T}_2^*$ and $\mathcal{T}_3^*$ refer to the sub-trajectories that end in the respective final leaf of the solution tree.

analyze the dependence of the trajectory probabilities on parameter distributions, we assume normal densities for k_{ij}, *Gamma* densities for γ_i, and uniform distributions for θ_{ij} in accordance with the modeling assumptions, and we consider four cases that differ for the expected values of the normal densities assigned to k_{ij} (Table 3.1).

The results in Table 3.1 are obtained with the standard Monte Carlo integration, considering 10^6 samples for each inequality system to evaluate. They highlight the dependence of trajectory probabilities on the expected values of k_{ij}. $P[\mathcal{T}_1]$ ranges from values close to 0 to values close to 1. Coherently with the inequality systems, $P[\mathcal{T}_1]$ increases, and $P[\mathcal{T}_2]+P[\mathcal{T}_3]$ decreases, while the expected value of $k_{10}+k_{11}+k_{12}$ in $\mathcal{V}_{15}$ (*i.e.*, the expected value of the *a priori* densities after restricting the support to $\mathcal{V}_{15}$) becomes higher than the expected value of $\gamma_1\theta_{12}$ in $\mathcal{V}_{15}$, and vice versa. In fact, at the first branching, T_{15}^{15} in $\mathcal{T}_1$ requires $k_{10}+k_{11}+k_{12} > \gamma_1\theta_{12}$, and T_{15}^{14} in $\mathcal{T}_2$ and $\mathcal{T}_3$ requires $k_{10}+k_{11}+k_{12} < \gamma_1\theta_{12}$. Hence, while the expected value of the left-hand side of the two reported inequalities increases in $\mathcal{V}_{15}$ with respect to the right-hand one, $P[\mathcal{T}_1]$ increases, and vice versa.

With regard to the number of useful samples, in all cases only a small part of the samples generated with the *a priori* densities belong to $\mathcal{V}_5$ (about 5%). Thus, a relevant part of the generated 10^6 samples is excluded from the evaluation of the probabilities. However, the number of useful parameters is such that the confidence interval of all of the estimated probabilities is always below 0.001.

4. An example from synthetic biology: the repressilator. In the word of [7]: *A general obstacle to the design of biochemical networks is the uncertainty about the values of parameters that characterize the interactions between different components.* Precise parameter values required in deterministic models lack the realistic variability that is inherent in every biological system. Then, in the context of model-based design for synthetic networks it is necessary to work with stochastic parameters.

Let us now consider a pioneering example in synthetic biology to show how the method proposed in this paper can provide a higher probability of a desired or undesired behavior by properly choosing network parameter distributions. More precisely, we consider a repressilator synthetic network in *Escherichia coli*, consisting of three

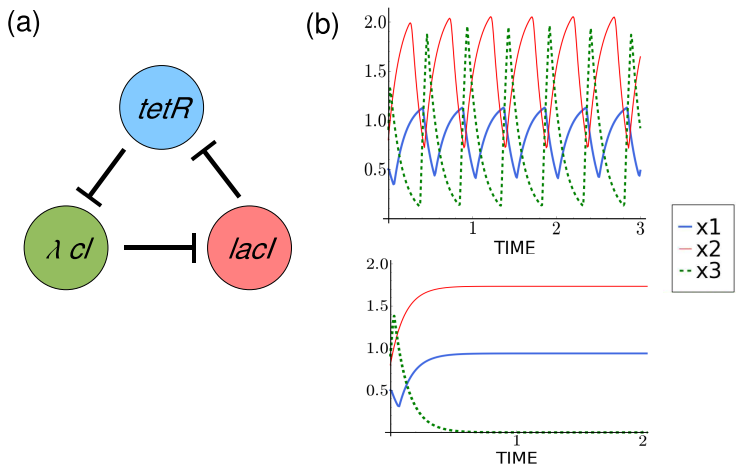

FIG. 4.1. *Three gene repressilator network implemented by Elowtiz and Leibler in [7]. (a) Schematic drawing of the network. (b) Temporal evolution of typical trajectories of (4.1). Numerical simulations were run in Berkeley Madonna, RK4 method with time-step=0.01 for initial* $x_i(0) = (0.5, 0.8, 0.9), (i = 1, 2, 3)$*, with the following parameters:* $q = 0.01$*,* $\theta_i = 1$*,* k_{i1}*=(8.35,15.42,29.34) and* γ_i*=(6.89,8.72,17.69) for oscillations (top) and* γ_i*=(8.89, 10.72,20.69) for stable trajectories (bottom).*

genes *lacI*, *tetR*, and *cI*, in which each gene represses its successor in a cycle [7]. Both experimental study and mathematical modeling confirm that the dynamical trajectories of this system can be classified into two types: either they converge to a steady state or they oscillate (Fig. 4.1).

We adapt the gene network to our framework (2.1) starting from its six-variable ODE model, with the only change of collapsing the translation into the transcription process. This results in a three-variable ODE model where each variable is associated with one threshold and the repression of a gene is represented by the $(1 - Z)$ term. The equations are given below:

$$\begin{aligned} \dot{x_1} &= k_{10} + k_{11}(1 - Z_{31}) - \gamma_1 x_1, \\ \dot{x_2} &= k_{20} + k_{21}(1 - Z_{11}) - \gamma_2 x_2, \\ \dot{x_3} &= k_{30} + k_{31}(1 - Z_{21}) - \gamma_3 x_3. \end{aligned} \tag{4.1}$$

We consider the scenario with no 'leakiness of the promoter' in this artificial system. Thus, we can ignore parameters k_{i0} (with $i = 1, 2, 3$) and let them equal to zero. Starting from the initial domain D_1 (in which $0 < x_i < \theta_{i1}$) with initial inequalities $k_{i1} > \gamma_i \theta_{i1}$, the simulation algorithm generates a solution tree with cyclic trajectories only. To obtain both types of dynamical behaviors, we relax the initial inequality on k_{31} by putting no restrictions. The result is a tree with five qualitative trajectories, three of which are cycles and two terminate in a stable point in D_3, in which $x_1 > \theta_{11}$ and x_2, x_3 as in D_1 (Fig. 4.2). The systems of inequalities from D_3 are mutually exclusive: $k_{31} < \gamma_1 \theta_{31}$ leads to a stable point in D_3, whereas $k_{31} > \gamma_1 \theta_{31}$ leads to D_{12}, in which $x_3 = \theta_{31}$ and x_1, x_2 as in D_3. The initial branching from D_1 consists of three not mutually alternative transitions whose probabilities are assigned by equally accounting for the non-empty intersections of ranges $\mathcal{V}_{D_1}^{D_2}$, $\mathcal{V}_{D_1}^{D_{10}}$ and $\mathcal{V}_{D_1}^{D_4}$ as described in Section 3.1.

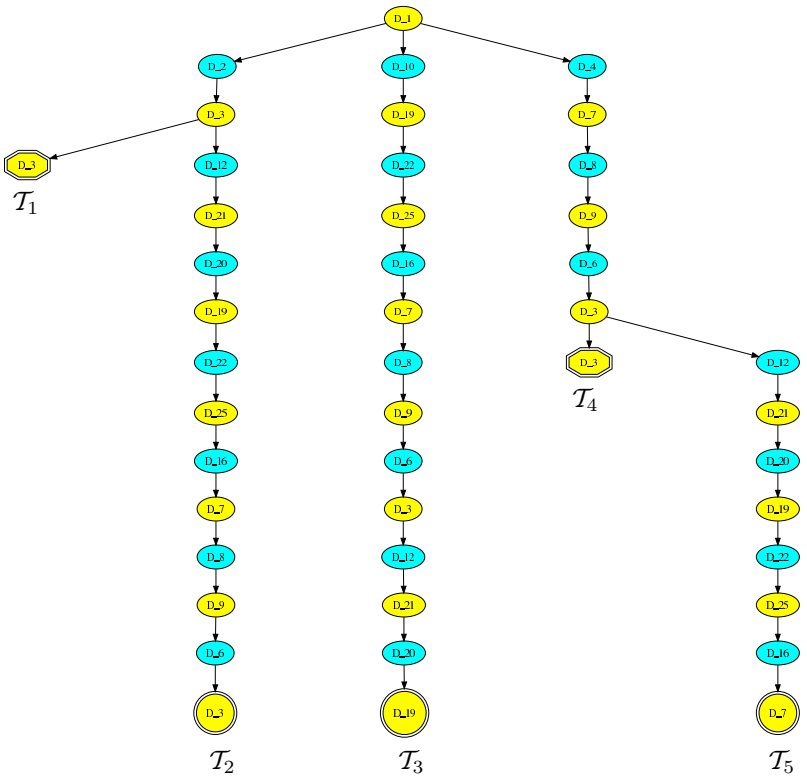

FIG. 4.2. *Solution tree of the repressilator network with initial inequalities* $k_{11} > \gamma_1\theta_{11}$ *and* $k_{21} > \gamma_2\theta_{21}$*. The tree shows the five possible trajectories generated starting from* D_1*; three trajectories are cycles* $(\mathcal{T}_2, \mathcal{T}_3, \mathcal{T}_5)$ *and two trajectories* $(\mathcal{T}_1, \mathcal{T}_4)$ *end as stable points in* D_3*.*

The probability of each trajectory in the tree is calculated by assigning a probability distribution to each model parameter. The probability of the occurrence of either a cyclic trajectory $P[\mathcal{T}_c]$ or a trajectory ending in a stable point $P[\mathcal{T}_s]$ is then obtained by properly summing up the probabilities of the trajectories in the tree. More precisely, $\mathcal{T}_2$, $\mathcal{T}_3$ and $\mathcal{T}_5$ are related to a cyclic behavior and $P[\mathcal{T}_c] = P[\mathcal{T}_2]+P[\mathcal{T}_3]+P[\mathcal{T}_5]$, and $\mathcal{T}_1$ and $\mathcal{T}_4$ end in a stable point and $P[\mathcal{T}_s] = P[\mathcal{T}_1]+P[\mathcal{T}_4]$. Obviously, $P[\mathcal{T}_c] + P[\mathcal{T}_s] = 1$.

For this network, we are in presence of very incomplete knowledge of parameter values, and we only know that all of them are positive. Following [7], we assume that all parameters of the same type are identically distributed in the *a priori* densities: production rates k_{11}, k_{21} and k_{31} are identically distributed, degradation rates γ_1, γ_2 and γ_3 are identically distributed, and thresholds θ_{11}, θ_{21} and θ_{31} are identically distributed. To start the stochastic analysis, we assign uniform distributions to all parameters. In all cases, we assume $\theta_{i1} \sim \mathcal{U}(0.7, 1.3)$, while different minimum and maximum values are explored for k_{i1} and γ_i. The results are reported in Table 4.1.

From these results we can provide a coarse stability diagram with stochastic parameters, where on the x-axis we report the production rate (k) and on the y-axis the degradation rate (γ) (Fig. 4.3a). The probability of obtaining a cycle gets its highest value in case (iv) and its lowest one in case (ii), and vice versa as for the probability for a trajectory to end in a stable point. Moreover, case (i) has almost

case	k_{i1}	γ_i	$P[\mathcal{T}_1]$	$P[\mathcal{T}_2]$	$P[\mathcal{T}_3]$	$P[\mathcal{T}_4]$	$P[\mathcal{T}_5]$	$P[\mathcal{T}_c]$	$P[\mathcal{T}_s]$
(i)	$\mathcal{U}(1,6)$	$\mathcal{U}(1,6)$	0.204	0.211	0.169	0.205	0.211	0.592	0.409
(ii)	$\mathcal{U}(1,6)$	$\mathcal{U}(6,10)$	0.487	0.014	0.007	0.487	0.005	0.026	0.974
(iii)	$\mathcal{U}(6,15)$	$\mathcal{U}(6,10)$	0.086	0.286	0.256	0.086	0.286	0.827	0.173
(iv)	$\mathcal{U}(6,15)$	$\mathcal{U}(1,6)$	0.002	0.333	0.332	0.002	0.333	0.997	0.003
(all)	$\mathcal{U}(1,15)$	$\mathcal{U}(1,10)$	0.125	0.262	0.226	0.124	0.262	0.751	0.249

TABLE 4.1

Probabilities of the occurrence of the simulated dynamics of the repressilator network in Fig. 4.2. The results are obtained by assigning uniform distributions to model parameters and by exploiting the standard Monte Carlo integration, with 10^6 generated samples for each probability. All confidence intervals of the estimated probabilities are below 0.001.

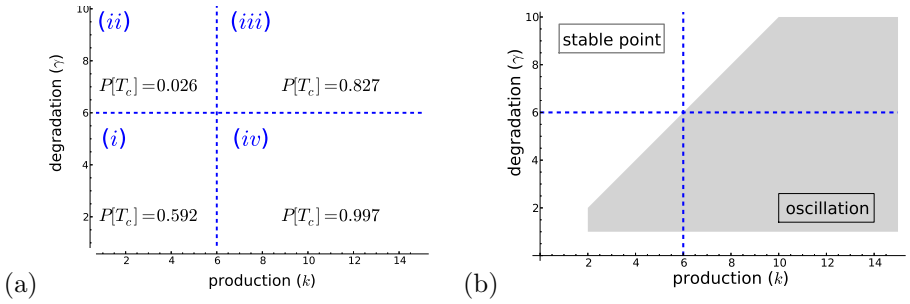

FIG. 4.3. *Phase diagrams of k versus γ in system (4.1). (a) Stability diagram with stochastic parameters where the probability of cyclic trajectories $P(\mathcal{T}_c)$ is reported in each region; dashed lines mark the boundary of the uniform probability distributions of γ and k for each case (i)-(iv), as described in Table 4.1. (b) Stability diagram generated by numerical integration of the* ODE *equations in Berkeley Madonna, RK4 method with $q = 0.01$, $\theta_i = 1$, and for each γ and k scanned with step 0.1 in $[1, 10]$ and $[1, 15]$, respectively. Values of k and γ taken in the grey or in the white region give rise, respectively, to oscillatory trajectories or stable trajectories.*

equal probabilities $P[\mathcal{T}_c]$ and $P[\mathcal{T}_s]$, and case (iii) has a higher probability $P[\mathcal{T}_c]$ that a cycle occurs.

To confirm our stochastic findings, we carry out numerical simulations to establish a stability phase diagram with k and γ as before (Fig. 4.3b). Let us observe that the latter diagram has the same structure and form as Fig.1b in [7], and matches the stochastic results, as expected.

To make a more refined phase diagram with stochastic parameters, we can further refine cases (i) and (iii) by either narrowing the range of the uniform distribution or changing the shape of the distribution.

To analyze how probabilities vary with distributions for parameters k_{i1} and γ_i, we consider a distribution with a different shape, and concentrated around a value in the uniform interval previously analyzed by adopting truncated Gaussian densities $\mathcal{TN}(\mu, \sigma^2, \alpha, \beta)$. Table 4.2 reports the results obtained by considering, by turns, truncated Gaussian densities concentrated in different peaks for one parameter and uniform distribution for the other. More precisely, we consider a uniform distribution for k_{i1} and truncated Gaussian densities for γ_i with different peaks for refining case (i), and the other way round for refining case (iii).

Coherently with the phase diagram (Fig. 4.3), it can be observed that in cases (i_a)-(i_d) $P[\mathcal{T}_c]$ increases while γ_i densities are concentrated close to the lower boundary (equal to 1) and decreases while they are concentrated close to the upper boundary (equal to 6). Similarly in cases (iii_a)-(iii_f), $P[\mathcal{T}_c]$ decreases while k_{i1} densities are

case	k_{i1}	γ_i	$P[\mathcal{T}_c]$	$P[\mathcal{T}_s]$
(i_a)	$\mathcal{U}(1,6)$	$\mathcal{TN}(2,4,1,6)$	0.703	0.297
(i_b)	$\mathcal{U}(1,6)$	$\mathcal{TN}(3,4,1,6)$	0.629	0.371
(i_c)	$\mathcal{U}(1,6)$	$\mathcal{TN}(4,4,1,6)$	0.551	0.450
(i_d)	$\mathcal{U}(1,6)$	$\mathcal{TN}(5,4,1,6)$	0.471	0.528
(iii_a)	$\mathcal{TN}(7,4,6,15)$	$\mathcal{U}(6,10)$	0.592	0.408
(iii_b)	$\mathcal{TN}(8,4,6,15)$	$\mathcal{U}(6,10)$	0.675	0.326
(iii_c)	$\mathcal{TN}(9,4,6,15)$	$\mathcal{U}(6,10)$	0.761	0.239
(iii_d)	$\mathcal{TN}(10,4,6,15)$	$\mathcal{U}(6,10)$	0.842	0.158
(iii_e)	$\mathcal{TN}(11,4,6,15)$	$\mathcal{U}(6,10)$	0.904	0.096
(iii_f)	$\mathcal{TN}(12,4,6,15)$	$\mathcal{U}(6,10)$	0.946	0.054

TABLE 4.2

Probabilities of the occurrence of the simulated cycles and trajectories ending in a stable point of the repressilator network in Fig. 4.2. The results are obtained by assigning a uniform distribution and a truncated Gaussian distribution, respectively, either to model parameters k_{i1} and γ_i (cases (i_a) - (i_d)) or to model parameters γ_i and k_{i1} (cases (iii_a) - (iii_f)), and by exploiting the standard Monte Carlo integration, with 10^6 generated samples for each transition probability.

concentrated close to the lower boundary (equal to 6) and increases while they are concentrated close to the upper boundary (equal to 15).

5. Discussion and conclusions. This paper deals with a method for assigning the probability of occurrence to the qualitative dynamics of gene regulatory models with steep sigmoid functions encompassed by (2.1) with given initial conditions. The initial state and parameters are not given a specific value but qualitatively and symbolically expressed through ranges of values defined in terms of order relations only. The full range of linear and nonlinear dynamics with different time scales is predicted by a simulation algorithm grounded on sound rules that implement the singular perturbation method adapted to the considered class of models. Each trajectory in the solution tree captures the qualitative properties of the network dynamics that depend only on the network structure and are invariant for ranges of parameter values that, in agreement with the initial ones, are symbolically calculated during the simulation.

The deterministic trajectories are then given a probability of occurrence by assigning a measurement of uncertainty to the parameter values. These are not equally known, and we can distinguish different scenarios where either all the parameter values are highly unknown or a subset, or the entire set, of parameter values are certain to some extent. Our method is able to integrate different levels of parameter knowledge from very incomplete to almost certain. In case of very incomplete knowledge, all parameter values are assumed to be uniformly distributed over their possible range of variability, or in other words they are assigned non-informative distributions, and the calculated probabilities derive from the sequence of parameter constraints and the multiple branching that characterize each single trajectory. When a certain knowledge is available, an informative distribution is assigned and is effectively used to compute the occurrence probability of the trajectories. The higher the knowledge of the network, the higher the number of coefficients with an informative distribution and the lower the standard deviation of these distributions. Parameter values with low variability increase accuracy and significance of the computed probabilities and contribute to better delimit those trajectories with a non-negligible probability to occur.

To get a complete view of the network dynamics by applying traditional numerical integrations of ODEs with stochastic coefficients is very hard and almost

impracticable. These methods provide one specific trajectory or subset of similar trajectories and, then, the integration should be repeated a great number of times with different coefficient configurations extracted from their respective density functions. However, also whenever a complete study is possible, the ranges of parameter values that characterize classes of qualitatively different behaviors need for post-processing to be identified. From a computational point of view, the ODE solution is computationally intensive, as it is iteratively performed on a discretized version of the equation by using Monte Carlo simulations or, in some cases, Markov Chain Monte Carlo methods, which require a high computational effort. In our case, probabilities are still calculated by a Monte Carlo integration. It still requires repetitions, but the computational burden for integrating a product of Bernoulli variables is extremely low in comparison to the effort required by the numerical solution of stochastic ODEs, so much so that standard Monte Carlo integration is sufficient to compute probabilities with reasonable computational times.

The herein proposed method is general, and it is applicable to study the dynamics of regulatory systems based on activation thresholds from application contexts, biological or not, other than natural or synthetic GRNs.

In the GRN context, the overall method can be used (1) to predict the full range of possible dynamics, along with their probability of occurrence, of a network in response to different perturbations or stimuli and finally (2) to develop control strategies aiming at leading the cellular system toward a desired state or away from an undesired state that may possibly be associated with a disease with the highest probability. Although methods exist for inferring the network structure from gene expression data, it currently finds its natural workbench in synthetic biology where the design of network structures with suitable connections and parameter constraints to produce a desired behavior is the key issue. The usefulness of our method comes from allowing the network designer to test different hypothesized network connections and from being able to give parameter suggestions also without prior knowledge. We think that it is progress to be able to provide relationships between parameters values (*i.e.*, inequalities) and the range of parameters to increase chances of desired (or undesired) behavior. However, physical or biological limitations could prohibit modification to the range of parameters; therefore, it might be more likely that certain parameter values happens at a higher probability than others. As we have shown on the gene repressilator system, a further control of the shape of the probability distribution could also fine-tune and additionally increase the probability of success. The automated control of both support and shape of probability distributions to maximize/minimize the occurrence probability of desired/undesired behaviors, quite challenging in the design context of synthetic networks, requires the development of optimization methods *ad hoc*.

Acknowledgements. We gratefully thank Diana X. Tran for useful general discussions on Synthetic Biology, and, in particular, on the repressilator system.

This work is carried out within the FLAGSHIP "InterOmics" project (PB.P05) that is funded and supported by the Italian MIUR and CNR organizations.

Appendix: Monte Carlo integration approach. The integral that gives the probability associated with a system of inequalities $d^{a,*}$, where * indicates the domain a transition occurs towards, is numerically computed by a repeated Monte Carlo sampling of the parameter set Ψ from its joint density function $f_a(\Psi)$. More precisely, a set $\Psi^{(c)}$ is generated at each sampling c, and the satisfaction $S^{(c)}$ of the

system $d^{a,*}$ for sample c is computed as:

$$S^{(c)} = \prod_{j=1}^{m} 1_{d_j^{a,*}\left(\Psi^{(c)}\right)}. \tag{5.1}$$

where $S^{(c)}$ is obviously equal only to 1 (system satisfied) or 0 (system not satisfied). The sampling process is repeated a high number of times n_s, and the expected value and the variance of $S^{(c)}$ are computed as follows:

$$E\left[S^{(c)}\right] = \frac{\sum_{c=1}^{n_s} S^{(c)}}{n_s}; \tag{5.2}$$

$$Var\left[S^{(c)}\right] = \frac{\sum_{c=1}^{n_s} \left(S^{(c)} - E\left[S^{(c)}\right]\right)^2}{n_s - 1}. \tag{5.3}$$

According to the central limit theorem, $E\left[S^{(c)}\right]$ is the estimator $\widehat{P}\left[d^{a,*}\right]$ of $P\left[d^{a,*}\right]$ and converges while n_s increases. The confidence interval of the estimator

$$\sigma_{\widehat{P}[d^{a,*}]} = \sqrt{\frac{Var\left[S^{(c)}\right]}{n_s}} \tag{5.4}$$

decreases while the number n_s of samples increases.

Operatively, the most simple way to sample Ψ from $f_a\left(\Psi\right)$ consists of extracting values ψ_i from their known *a priori* independent densities $f_i^{priori}\left(\psi_i\right)$. The resulting set $\Psi^{(c)}$ is exploited for the computation of the probability only if $\Psi^{(c)} \in \mathcal{V}_a$. Then, (5.2) is modified as follows:

$$E\left[S^{(c)}|Q^{(c)}\right] = \frac{\sum_{c=1}^{n_s} S^{(c)}Q^{(c)}}{\sum_{c=1}^{n_s} Q^{(c)}}, \tag{5.5}$$

where $Q^{(c)} = 1$ if $\Psi^{(c)} \in \mathcal{V}_a$, and $Q^{(c)} = 0$ elsewhere. Coherently:

$$\sigma_{\widehat{P}[d^{a,*}]} = \sqrt{\frac{\sum_{c=1}^{n_s} \left[\left(S^{(c)} - E\left[S^{(c)|Q^{(c)}}\right]\right)^2 Q^{(c)}\right]}{\sum_{c=1}^{n_s} Q^{(c)} \left[\left(\sum_{c=1}^{n_s} Q^{(c)}\right) - 1\right]}}. \tag{5.6}$$

The number n_{us} of *useful samples*, *i.e.* those with $Q^{(c)} = 1$, is in general lower than the n_s generated ones but, in most cases, the ratio n_{us}/n_s is adequate to get an acceptable convergence rate of the Monte Carlo integration. This is not the case when $n_{us} \ll n_s$. In the latter case, two variants of the Monte Carlo integration can be considered to make the converge rate faster, namely the importance sampling and the sequential sampling [20, 28]. Whereas the latter variant can still work on the same equation (3.2) as the standard approach, the former one operates on a modified equation that in our framework can be obtained as suggested in the following.

The samples for evaluating the current transition T_a^b are generated in accordance with a new density function $g_a\left(\Psi\right)$, which is concentrated around the expected value of samples in $\mathbf{\Sigma}$, where $\mathbf{\Sigma}$ is the set of samples with $|\mathbf{\Sigma}| = m_s$, evaluated in the previous transition for which $S^{(c)} = 1$, and $Q^{(c)} = 1$. In detail, a normal probability

density function $h_{a,i}(\psi_i)$ is introduced for each $\psi_i \in \Psi$, with expected value μ_i and variance σ_i^2:

$$\mu_i = \frac{1}{m_s}\sum_{j=1}^{m_s}\psi_i^{(c_j)} \qquad \sigma_i^2 = \eta\frac{\sum_{j=1}^{m_s}\left(\psi_i^{(c_j)} - \mu_i\right)^2}{m_s - 1}$$

where η is a scaling coefficient for variance and samples $\psi_i^{(c_j)}$ are taken from $\mathbf{\Sigma}$. The densities $h_{a,i}(\psi_i)$ are independent, and their product defines the joint probability density function $h_a(\Psi)$. Finally, we define $g_a(\Psi)$ as a mixture between $h_a(\Psi)$ and the original $f_a(\Psi)$ over $\mathcal{V}_a$:

$$g_a(\Psi) = \begin{cases} \frac{\omega f_a(\Psi)+(1-\omega)h_a(\Psi)}{\int_{\mathcal{V}_a}[\omega f_a(\Psi)+(1-\omega)h_a(\Psi)]d\psi_1\ldots d\psi_{n_c}} & \Psi \in \mathcal{V}_a \\ 0 \qquad\qquad elsewhere \end{cases} \tag{5.7}$$

where the weight $\omega \in [0,1]$ allows us to balance the mixture.

The conditional probability of (3.2) is then modified as follows:

$$P[d^{a,*}] = \int_{\mathcal{V}_a}\left[\frac{f_a(\Psi)}{g_a(\Psi)}\prod_{j=1}^{m}1_{d_j^{a,*}(\Psi)}\right]g_a(\Psi)\,d\psi_1\ldots d\psi_{n_c}. \tag{5.8}$$

The denominators of $f_a(\Psi)$ and $g_a(\Psi)$, reported in (3.7) and (5.7), respectively, are computed with a Monte Carlo sampling and, then, the computation of (5.8) is carried out with a further sampling. Although three integrals have to be computed, the importance sampling is computationally more convenient than the standard Monte Carlo sampling in the case of rare event simulation with $n_{us} \ll n_s$, as it requires a lower number of generated samples to reach the same convergence of the estimation, *i.e.*, the same $\sigma_{\widehat{P}[d^{a,*}]}$ [20, 28].

REFERENCES

[1] U. Alon, *Introduction to Systems Biology: Design Principles of Biological Circuits*, Chapman & Hall, Boca Raton, FL, 2007.

[2] Frank J. Bruggeman and Hans V. Westerhoff, *The nature of systems biology*, Trends in Microbiology, 15 (2007), pp. 45–50.

[3] Y. Cao and D. C. Samuels, *Discrete stochastic simulation methods for chemically reacting systems*, Methods in Enzymology, 454 (2009), pp. 115–140.

[4] H. de Jong, *Modeling and simulation of genetic regulatory systems: A literature review*, Journal of Computational Biology, 9 (2002), pp. 67–104.

[5] Hidde de Jong, Johannes Geiselmann, Céline Hernadez, and Michel Page, *Genetic network analyzer: qualitative simulation of genetic regulatory networks*, Bioinformatics, 19 (2003), pp. 336–344.

[6] Samuel Drulhe, Giancarlo Ferrari-Trecate, and Hidde de Jong, *The switching threshold reconstruction problem for piecewise affine models of genetic regulatory networks*, IEEE Transactions on Automatic Control, 53 (2008), pp. 153–165.

[7] Michael B. Elowitz and Stanislas Leibler, *A synthetic oscillatory network of transcriptional regulators*, Nature, 403 (2000), pp. 335–337.

[8] D. T. Gillespie, *A general method for numerically simulating the stochastic time evolution of coupled chemical reactions*, Journal of Computational Physics, 22 (1976), pp. 403–434.

[9] ———, *Exact stochastic simulation of coupled chemical reactions*, The Journal of Physical Chemistry, 81 (1977), pp. 2340–2361.

[10] ———, *Approximate accelerated stochastic simulation of chemically reacting systems*, Journal of Chemical Physics, 115 (2001), pp. 1716–1733.

[11] L. H. Hartwell, J. J. Hopfield, S. Leibler, and A. W. Murray, *From molecular to modular cell biology*, Nature, 402 (1999), pp. C47–C52.

[12] Matthias Heinemann and Sven Panke, *Synthetic biology – putting engineering into biology*, Bioinformatics, 22 (2006), pp. 2790–2799.

[13] Liliana Ironi and Luigi Panzeri, *A computational framework for qualitative simulation of nonlinear dynamical models of gene-regulatory networks*, BMC Bioinformatics, 10(Suppl. 12: S14) (2009).

[14] Liliana Ironi, Luigi Panzeri, Erik Plahte, and Valeria Simoncini, *Dynamics of actively regulated gene networks*, Physica D: Nonlinear Phenomena, 240 (2011), pp. 779–794.

[15] Liliana Ironi and Diana X. Tran, *A simulator of the nonlinear dynamics of gene-regulatory networks*, tech. report, IMATI-CNR (*in preparation*), 2013.

[16] Guy Karlebach and Ron Shamir, *Modelling and analysis of gene regulatory networks*, Nature Reviews Molecular Cell Biology, 9 (2008), pp. 770–780.

[17] Douglas B. Kell, *Metabolomics, modelling and machine learning in systems biology–towards an understanding of the languages of cells*, Febs Journal, 273 (2006), pp. 873–894.

[18] A. S. Khalil and J. J. Collins, *Synthetic biology: applications come of age*, Nature Reviews Genetics, 11 (2010), pp. 367–379.

[19] Peter E. Kloeden and Eckhard Platen, *Numerical solution of stochastic differential equations*, Springer, Berlin, 1992.

[20] Dirk P. Kroese, Thomas Taimre, and Zdravko I. Botev, *Handbook of Monte Carlo methods*, Wiley Series in Probability and Statistics, 2011.

[21] D. Kulasiri, L. K. Nguyen, S. Samarasinghe, and Z. Xie, *A review of systems biology perspective on genetic regulatory networks with examples*, Current Bioinformatics, 3 (2008), pp. 197–225.

[22] A. Machina, R. Edwards, and P. van den Driessche, *Singular dynamics in gene network models*, SIAM Journal on Applied Dynamical Systems, 12 (2013), pp. 95–125.

[23] H. H. McAdams and A. Arkin, *Stochastic mechanisms in gene expression*, Proceedings of the National Academy of Sciences USA, 94 (1976), pp. 814–819.

[24] Bernt Øksendal, *Stochastic differential equations: an introduction with applications - 6th Edition*, Springer, Berlin, 2003.

[25] Pawel Paszek, *Modeling stochasticity in gene regulation: Characterization in the terms of the underlying distribution function*, Bulletin of Mathematical Biology, 69 (2007), pp. 1567–1601.

[26] Erik Plahte and Sissel Kjøglum, *Analysis and generic properties of gene regulatory networks with graded response functions*, Physica D: Nonlinear Phenomena, 201 (2005), pp. 150–176.

[27] Oliver Purcell, Nigel J. Savery, Claire S. Grierson, and Mario di Bernardo, *A comparative analysis of synthetic genetic oscillators*, Journal of the Royal Society Interface, 7 (2010), pp. 1503–1524.

[28] Gerardo Rubino and Bruno Tuffin, *Rare event simulation using Monte Carlo methods*, John Wiley & Sons, Ltd., 2009.

[29] Siren R. Veflingstad and Erik Plahte, *Analysis of gene regulatory network models with graded and binary transcriptional responses*, Biosystems, 90 (2007), pp. 323–339.